IEEE Access
Multidisciplinary | Rapid Review | Open Access Journal

SPECIAL SECTION ON MILLIMETER-WAVE AND TERAHERTZ PROPAGATION, CHANNEL MODELING AND APPLICATIONS

Received March 26, 2019, accepted May 1, 2019, date of publication May 6, 2019, date of current version May 17, 2019.

Digital Object Identifier 10.1109/ACCESS.2019.2915035

OFDM-OAM Modulation for Future Wireless Communications

TAO HU[1], (Student Member, IEEE), YANG WANG[1], (Member, IEEE), XI LIAO[1], (Member, IEEE), JIE ZHANG[1,2], (Senior Member, IEEE), AND QILONG SONG[1]

[1]School of Communication and Information Engineering, Chongqing University of Posts and Telecommunications, Chongqing 400065, China
[2]Department of Electronic and Electrical Engineering, The University of Sheffield, Sheffield S10 2TN, U.K.

Corresponding author: Yang Wang (wangyang@cqupt.edu.cn)

This work has been supported in part by the National Natural Science Foundation of China under Grant 61601073, in part by the High-end Project for Doctoral Students at Chongqing University of Posts and Telecommunications under Grant BYJS201801 and in part by the European Union's Horizon 2020 research and innovation programme-is3DMIMO under Grant 734798.

ABSTRACT Orbital angular momentum (OAM) has attracted considerable attention as a novel solution for wireless communications because its orthogonal modes significantly increase the channel capacity without an additional frequency band. The joint multiplexing between OAM technologies and other modulation techniques has not been thoroughly investigated. In this paper, we first proposed the orthogonal frequency-division multiplexing-orbital angular momentum (OFDM-OAM) multiple-input-multiple-output (MIMO) system. The proposed OFDM-OAM MIMO based on the discrete Fourier transformation (DFT) operations achieves a very high sum-rate and spectrum efficiency (SE). However, the expensive hardware and software overheads for transmitting and receiving OAM waves lead to an unexpected cost for the OFDM-OAM MIMO scheme. A time-switched OFDM-OAM (TOO) MIMO is then proposed to reduce the computational complexity, and the procedure of OAM generations and recoveries has also explicitly been derived. The mathematical derivation shows that the proposed TOO MIMO system based on a simple switching sequence is suitable for small-scale and low-cost wireless broadband communications, and the simulation results demonstrate that the TOO MIMO scheme achieves a considerable SE and much less computational complexity than the OFDM-OAM MIMO scheme.

INDEX TERMS Orbital angular momentum (OAM), joint multiplexing, orthogonal frequency-division multiplexing-orbital angular momentum (OFDM-OAM), multiple-input multiple-output (MIMO), spectrum efficiency (SE), time-switched OFDM-OAM (TOO).

I. INTRODUCTION

Massive multiple-input-multiple-output (MIMO), as one of the fundamental techniques for the fifth generation of mobile wireless communication systems, refers to the case in which unlimited numbers of antennas are integrated within a base station (BS) [1]. With the implementation of massive MIMO techniques, substantial capacity is provided by fully utilizing the spatial degrees of freedom. However, many practical challenges need to be solved in massive MIMO communications, for instance, high hardware integration in BSs and high-complexity baseband processing in transmitters. Also, the 3D (three-dimensional) massive MIMO technique has been proposed to exploit an additional degree of freedom (in the vertical plane) due to the realistic 3D radio propagation environment [2], [3]. Multiple users in different vertical directions at the same horizontal directions can be distinguished in 3D massive MIMO communication systems, and extra flexibility in interference management can be obtained. The interference could be significantly decreased rather than entirely eliminated by using these MIMO techniques; therefore, maximizing the channel capacity of MIMO systems is a crucial issue in wireless transmissions.

Compared with the degrees of freedom offered by conventional MIMO systems in the temporal, frequency and spatial dimensions, orbital angular momentum (OAM) or radio vortex technology exploits a brand-new dimension, i.e., the mode division multiplexing MIMO (MDM-MIMO) for line-of-sight (LOS) wireless communications, where the capacity can be maximized in a LOS scenario due to the characteristic of orthogonality between different integer modes, and only the integer modes are suitable for propagations, which are

The associate editor coordinating the review of this manuscript and approving it for publication was Yi Fang.

the eigenmodes [4]–[10]. Therefore, the OAM techniques can be widely applied to information exchanges in the data center, unmanned aerial vehicle (UAV) air-to-ground communications, and wireless backhaul communications due to the superiority in LOS communications.

It is well known that the multiplexing of OAM waves with different eigenmodes can achieve high capacity and spectrum efficiency (SE). In optical communications, the researchers have obtained outstanding achievements in recent years [11]–[15]. Besides, considerable attention has been focused on OAM wireless communications [16]–[24]. The OAM technology was first applied to wireless communication at low frequency ($\leq$ 1GHz) in [16], and then the first OAM experimental research was conducted to prove the feasibility of OAM-based wireless communication [17]. In [20]–[24], the researchers theoretically analyze the feasibility of OAM wireless communications. The researchers of [25] proposed radio vortex-multiple-input multiple-output communication (RV-MIMO) systems, which can achieve a very high capacity gain over the conventional MIMO systems in free space. Considering an ideal LOS wireless transmission environment, the researchers in [26] proposed an OAM-embedded-massive MIMO (OEM) system that dramatically improves the spectrum efficiency (SE) in the millimeter wave band. Since OAM-carrying waves with different eigenmodes are mutually orthogonal in coaxial transmission scenarios, MDM techniques are capable of achieving high channel capacity without an additional frequency band in an OAM-MDM communication experiment at a frequency of 10 GHz [27]. In [28], an OAM-based millimeter wave communication system with high-capacity and low-complexity was proposed, which is suitable for short-range backhaul links and data center with large bandwidth. Then, an OAM spatial modulation (OAM-SM) system was introduced in [29], which is suitable for long-range communications due to its strong robustness against transmission attenuations. Considering a misalignment case, the work in [30] shown that a suitable beam steering vector could be designed to address the problems in both non-parallel and off-axis cases. The researchers in [31] demonstrated that the channel capacity of OAM-based MIMO communication systems could be enhanced by employing a more significant number of antenna elements in the receiver than in the transmitter. Besides, an adaptive mode modulation (AMM) scheme with Huffman coding was proposed in [32] to improve significantly the SE of the OAM-based communication systems.

However, in the recent researches on OAM wireless communications, the joint multiplexing between OAM techniques and other modulation techniques such as spatial modulation, polarization modulation and orthogonal frequency-division multiplexing (OFDM) are barely considered. Thus, the assessment for system performance of the joint multiplexing technology would be an important issue.

The OFDM techniques for treating frequency-selective fading can perfectly multiplex with the OAM technologies; furthermore, both OFDM and OAM can be realized in the baseband by spatial-domain and time-domain IDFT operators. The authors in [33] proposed a 2-D FFT-based OAM-OFDM transceiver with low computational complexity for wireless communications. Based on the research in [33], we detailly derived the channel model of the orthogonal frequency-division multiplexing-orbital angular momentum (OFDM-OAM) system, and then proposed a time-switched OFDM-OAM (TOO) MIMO system continued by analyzing the SE of the TOO MIMO system. The simulation results indicate that the SE of the proposed TOO MIMO communication system encounters a performance loss in short range. For a normal far field communication distance, fortunately, the TOO MIMO system achieves a significant performance over both the OFDM-OAM MIMO and the conventional MIMO systems with the increase of transmission distance. Besides, the proposed OFDM-OAM transmitter/receiver based on radio frequency (RF) switches considerably decreases the overhead in hardware.

The remainder of this paper is organized as follows. Section II introduces the OFDM-OAM MIMO communication system and the TOO MIMO communication system. The specific mathematical analysis of channel capacity for TOO MIMO communication systems is derived in Section III. Then, the numerical results in Section IV evaluate the SE of the proposed TOO MIMO communication system compared with OFDM-OAM MIMO and the conventional MIMO communication systems. Finally, conclusions are drawn in Section V.

II. SYSTEM MODEL

The MDM-MIMO wireless communication system model is shown in Fig. 1, where the transmit uniform circular arrays (UCAs) are equipped with N_t antenna elements and the receive UCAs are equipped with N_r antenna elements. The MDM-MIMO system has additional OAM eigenmodes for multiplexing transmission and demultiplexing receiving, which could be realized by a phase-shifter networking or DFT/IDFT operator.

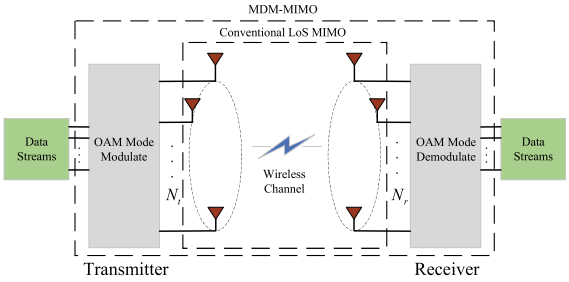

FIGURE 1. System models of the MDM-MIMO and the conventional LOS MIMO wireless communications.

A. CONVENTIONAL MIMO

In a conventional LOS MIMO communication model, the complex channel gain between the n^{th} transmitting

antenna and the m^{th} receiving antenna is given by

$$h_{mn} = \frac{\eta}{d_{mn}} e^{-jkd_{mn}}. \tag{1}$$

where $\eta = \frac{\beta\lambda}{4\pi}$ is a constant corresponding to the attenuation, in which λ is the wavelength, $k = 2\pi/\lambda$ is the wavenumber, and d_{mn} is the transmission distance from the n^{th} transmitting element to the m^{th} receiving element, which can be calculated as

$$d_{mn} = \sqrt{D^2 + R_t^2 + R_r^2 - 2R_t R_r \cos\theta_{mn}}. \tag{2}$$

where D is the distance between the transmit UCAs and the receive UCAs, $\theta_{mn} = 2\pi\left(\frac{m}{N_r} - \frac{n}{N_t}\right)$ is the rotation angle between the m^{th} receiving element and the n^{th} transmitting element, and R_t and R_r are the radii of the transmit UCAs and the receive UCAs, respectively.

Assuming that the mutual coupling between each antenna element can be neglected, the $N_r \times N_t$ MIMO channel matrix $\mathbf{H}$ can be expressed as

$$\mathbf{H} = \eta \begin{bmatrix} \frac{e^{-jkd_{11}}}{d_{11}} & \frac{e^{-jkd_{12}}}{d_{12}} & \cdots & \frac{e^{-jkd_{1N_t}}}{d_{1N_t}} \\ \frac{e^{-jkd_{21}}}{d_{21}} & \frac{e^{-jkd_{22}}}{d_{22}} & \cdots & \frac{e^{-jkd_{2N_t}}}{d_{2N_t}} \\ \vdots & \vdots & \ddots & \vdots \\ \frac{e^{-jkd_{N_r1}}}{d_{N_r1}} & \frac{e^{-jkd_{N_r2}}}{d_{N_r2}} & \cdots & \frac{e^{-jkd_{N_rN_t}}}{d_{N_rN_t}} \end{bmatrix}. \tag{3}$$

All the entries of $\mathbf{H} \in \mathbb{C}^{N_r \times N_t}$ are nonzero as described in the above equation; therefore, the conventional LOS MIMO communication system will encounter a very high interchannel interference (ICI). To address this problem, some equalization algorithms need to be designed to cancel the ICI at the receiver, whereas in an ideal MDM-MIMO system, the ICI could be eliminated. Since the specific derivation of MDM-MIMO system has been given in [24], [25], [27] and [29], it will not be covered in this paper.

B. OFDM-OAM MIMO

For a LOS MIMO system with N_t-element UCAs at the transmitter and N_r-element UCAs at the receiver, an OFDM-OAM transmitter could be implemented by a fully digital method in baseband, and the specific process can be divided into two stages, as follows:

1) OFDM FREQUENCY MODULATION

original information symbols are modulated into M groups of OFDM signals by performing an M-point inverse discrete Fourier transform (IDFT) in the frequency domain.

2) OAM EIGENMODE MODULATION

by performing an N_t-point IDFT in the spatial domain, each group of the OFDM information symbols could be modulated into at most N_t OAM signals with different eigenmodes.

The OFDM signal, which can be obtained by adding a subcarrier signal to the original signal, is given by

$$v(t, f) = s(t)\, e^{j2\pi ft}. \tag{4}$$

where $s(t)$ is a conventional radio signal, f is frequency of the OFDM subcarrier. Similarly, the vortex signal combines OAM and electromagnetic waves, which can be obtained by adding a helical phase factor $e^{jl\varphi}$ to a conventional electromagnetic wave signal. Electromagnetic wave fronts rotate around the directions of propagation in the given LOS MIMO system; therefore, the vortex signal is given by

$$v(t, \phi) = s(t)\, e^{jl\phi}. \tag{5}$$

where ϕ is the azimuth angle between transmit UCAs and receive UCAs, and l is the OAM eigenmode. From Eq. (4) and (5), the OFDM radio vortex with eigenmode l and frequency f can be generated by feeding each antenna element in the transmit UCAs with

$$a_{l,f} = \frac{p_{l,f}}{\sqrt{N_t M}} x_{l,f} e^{j2\pi\left[\frac{(n-1)l}{N_t} + \frac{(m-1)f}{M}\right]} \tag{6}$$

where $p_{l,f}$ is the power allocation factor of the information symbol $x_{l,f}$. The transmitter can generate multiple OFDM-OAM signals with different eigenmodes and subcarriers simultaneously in an OFDM-OAM MIMO system; therefore, the total excitation on the n^{th} transmitter element becomes the linear superposition of the current that is fed for each independent eigenmode and subcarrier. Thus, the total excitation in the OFDM-OAM MIMO system becomes

$$a = \sum_{l\in\mathcal{L}} \sum_{f\in\mathcal{F}} \frac{p_{l,f}}{\sqrt{N_t M}} x_{l,f} e^{j2\pi\left[\frac{(n-1)l}{N_t} + \frac{(m-1)f}{M}\right]} \tag{7}$$

$\mathcal{L} = \{-N_t/2, \ldots, 0, 1, \ldots, N_t/2 - 1\}$ is the set of OAM eigenmodes, and $\mathcal{F} = \{f_0, f_1, \ldots, f_{M-1}\}$ is the set of OFDM subcarriers. Thus, the matrix form of the transmitted symbols would be described as

$$\mathbf{a} = \mathbf{F}_{N_t}^H \mathbf{P} \mathbf{s} \mathbf{F}_M^H. \tag{8}$$

where $\mathbf{P} = \mathrm{diag}\left(\left[P_0, P_1, \cdots, P_{N_t-1}\right]\right)$ is the power allocation matrix, $\mathbf{s} = [\mathbf{s}(1), \mathbf{s}(2), \cdots, \mathbf{s}(M)]$ are the $N_t \times M$ original information symbols block, $\mathbf{F}_M^H$ and $\mathbf{F}_{N_t}^H$ are the M-point and N_t-point IDFT matrixes, respectively. Note that $(\cdot)^H$ denotes the conjugate transpose operation, and the $[m, n]$th entry of an N-point DFT matrix $\mathbf{F}_N$ satisfies

$$t[m, n] = \frac{1}{\sqrt{N}} e^{-j2\pi\frac{(m-1)(n-1)}{N}}. \tag{9}$$

The transmission signals can be recovered by performing an N_r-point DFT for OAM mode demodulation and an additional M-point DFT for OFDM demodulation, and these baseband IDFT/DFT processing procedures are realized by performing FFT algorithms in a field-programmable gate array (FPGA) or digital signal processor (DSP). Thus,

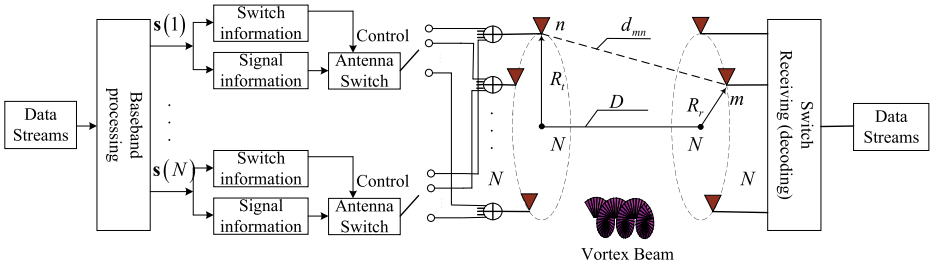

FIGURE 2. The architecture of the TOO MIMO transceiver implemented by radio switches.

the outputs of the receiver array corresponding to eigenmode l_r and subcarrier f_r are given by

$$r_{l_r,f_r} = \frac{1}{\sqrt{N_r M}} \sum_{p=0}^{N_r-1} \sum_{q=0}^{M-1} b_{l_r,f_r} e^{-j2\pi\left(\frac{pl_r}{N_r}+\frac{qf_r}{M}\right)} \tag{10}$$

where b_{l_r,f_r} is the received information symbol. Thus, the output matrix is defined as

$$\mathbf{r} = \mathbf{F}_{N_r}\mathbf{b}\mathbf{F}_M \tag{11}$$

with

$$\mathbf{b} = \mathbf{H}\mathbf{a} + \mathbf{n} \tag{12}$$

where $\mathbf{r}\in^{N_r\times M}$ is the received signal matrix, additive white noise matrix $\mathbf{n}\in^{N_r\times M}$ satisfies $E\left\{\mathbf{n}\mathbf{n}^H\right\} = \sigma_n^2\mathbf{I}_{N_r}$, and $\mathbf{H} \in^{N_r\times N_t}$ is the free-space LOS MIMO channel matrix. According to (8), (12) and (13) above, we have

$$\mathbf{r} = \mathbf{F}_{N_r}\mathbf{H}\mathbf{F}_{N_t}^H\mathbf{P}\mathbf{s}\mathbf{F}_M^H\mathbf{F}_M + \mathbf{F}_{N_r}\mathbf{n}\mathbf{F}_M \tag{13}$$

where $\mathbf{H}_{\mathrm{OAM}} = \mathbf{F}_{N_r}\mathbf{H}\mathbf{F}_{N_t}^H$ is the OAM channel. For m^{th} OFDM subcarrier, the $N_r \times 1$ demodulated OFDM-OAM signal vector is given by

$$\mathbf{r}(m) = \mathbf{H}_{\mathrm{OFDM-OAM}}^m\mathbf{a}(m) + \widehat{\mathbf{n}}(m) \tag{14}$$

where $\mathbf{H}_{\mathrm{OFDM-OAM}}^m$ is the OFDM-OAM subchannel, expressed as

$$\mathbf{H}_{\mathrm{OFDM-OAM}}^m = \mathbf{F}_{N_r}\mathbf{H}(m)\mathbf{F}_{N_t}^H \tag{15}$$

with

$$\mathbf{H}(m) = \frac{1}{\sqrt{M}}\mathbf{H}e^{-j\frac{2\pi m}{M}} \tag{16}$$

where $\mathbf{H}(m)$ is the OAM frequency-domain channel.

C. TIME-SWITCHED OFDM-OAM (TOO) MIMO

It is clear that the number of OAM eigenmodes depend on the number of antenna elements at the transmitter; thus, the computational complexity of modulation/demodulation of OFDM and OAM could be extraordinary high when the sets of $\mathcal{L}$ and $\mathcal{F}$ take large value. In UCAs-based transmitter, the binary switches can replace the phase shift units; therefore, the phase differences of OAM wavefront can be generated by feeding the same information symbols to UCAs where only one antenna element is active in each time slot. Also, the authors in [34] have proposed a time-variant MIMO receiver which proves the feasibility of spatial multiplexing based on switches.

As shown in Fig. 2, we employ time-switched uniform circular arrays (TS-UCAs) in the transmitter to generate multiple OAM eigenmodes with different carrier frequencies simultaneously to reduce the complexity of baseband processing. Moreover, the examples of 4-element time-switched patterns for single and numerous RF chains are shown in Fig. 3 (a) and (b), where both the time and antenna resources are divided into $N_t = 4$ resource blocks. For the i^{th} $(1 \le l \le N_t)$ time slot, a_n $(1 \le n \le N_t)$ indicates the n^{th} antenna element, and $t_s = t_{\mathrm{off}}^n - t_{\mathrm{on}}^n$ denotes the duration of n^{th} antenna switch-ON corresponding to the i^{th} time slot where t_{on}^n and t_{off}^n are the time of antenna-ON and the time of antenna-OFF, respectively. For a single data stream, in Fig. 3 (a), only one antenna element is switch-ON in each time slot. And in this case, only one RF chain is needed for transmission. In Fig. 3 (b), all the antenna elements are switch-ON to transmit multiple data streams independently in each time slot, where a total of 4 RF chains are required (the conventional multi-user MIMO systems). Compared with the OFDM-OAM MIMO system which is implemented by IDFT operations at baseband, moreover, the TOO scheme can significantly reduce the hardware overhead in OAM/OFDM modulation by using RF switches.

1) GENERATION OF THE VORTEX SIGNAL

We consider an N_t-element UCAs with radius R; thus, the steering vector $\mathbf{a}_N(\phi)$ can be described as

$$\mathbf{a}_N(\phi) = \left[e^{-j\phi_0(\psi,\varphi)},\ e^{-j\phi_1(\psi,\varphi)},\ \cdots\ e^{-j\phi_{N_t-1}(\psi,\varphi)}\right] \tag{17}$$

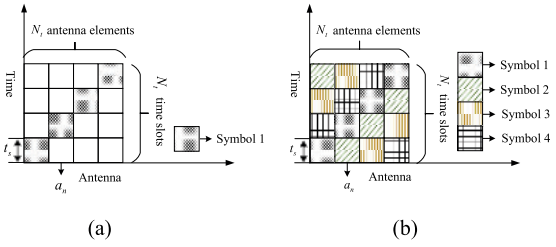

FIGURE 3. Time-switched patterns of 4-element: (a) single data stream; (b) multiple data streams.

with

$$\phi_n(\psi,\varphi) = -\frac{2\pi}{\lambda} R\sin(\psi)\cos\left(\varphi - \frac{2\pi n}{N_t}\right) \tag{18}$$

where $\phi_n(\psi,\varphi)$ denotes the skewing between the n^{th} element and the reference element, and ψ and φ are the elevation angle and the azimuth angle in the transmitter, respectively.

TS-UCAs employ simple RF switches to feed the antenna elements. A suitable time-switched sequence can be designed to offer a corresponding phase difference for each component, replacing many of the expensive phase shift units. Hence, for m^{th} data stream, the output of the TS-UCAs can be modeled as

$$x_m(\psi,\varphi,t) = \sum_{n=0}^{N_t-1} s_n(m)e^{j2\pi ft} \times e^{j\frac{2\pi}{\lambda}R\sin(\psi)\cos\left(\varphi-\frac{2\pi n}{N_t}\right)} I_n(t). \tag{19}$$

where $s_n(m)e^{j2\pi ft}$ is the m^{th} conventional radio signal corresponding to frequency f at the n^{th} antenna element, λ is the wavelength, and $I_n(t)$ is the time-switched sequence, which can be written as

$$I_n(t) = \begin{cases} 1 & kT_s + t_{\text{on}}^n \le t < kT_s + t_{\text{off}}^n \\ 0 & \text{others} \end{cases}. \tag{20}$$

where k is an integer and T_s is the period of total N_t switching sequences. The Fourier expansion of $I_n(t)$ is given by

$$I_n(t) = \sum_{l=-\infty}^{\infty} S_n^l e^{j\frac{2\pi lt}{T_s}} \tag{21}$$

with

$$S_n^l = \frac{1}{T_s}\int_0^{T_s} I_n(t)e^{-j\frac{2\pi lt}{T_s}}dt \tag{22}$$

where l denotes the order of the Fourier series (it also means the eigenmode of the OAM beam in this paper), and its Fourier expansion corresponding the l^{th} harmonic coefficient is driven by

$$S_n^l = \frac{\sin\left[\pi l\left(\tau_{\text{off}}^n - \tau_{\text{on}}^n\right)\right]}{\pi l} e^{-j\pi l(\tau_{\text{off}}^n + \tau_{\text{on}}^n)} \tag{23}$$

Thus, the output signal has the new expression

$$x_m(\psi,\varphi,t) = \sum_{l=-\infty}^{\infty} A(l)\, e^{j2\pi l f_s t} \times \sum_{n=0}^{N_t-1} s_n(m)e^{2\pi ft}e^{-jl\Theta_n}e^{j\phi_n(\psi,\varphi)} \tag{24}$$

where $A(l) = \frac{\sin[\pi l(\tau_{\text{off}}^n - \tau_{\text{on}}^n)]}{\pi l}$ is the amplitude of the l^{th} harmonic signal, $\Theta_n = \pi\left(\tau_{\text{off}}^n + \tau_{\text{on}}^n\right)$ is the phase difference between the n^{th} element and original element, $\phi_n(\psi,\varphi) = \frac{2\pi}{\lambda}R\sin(\psi)\cos\left(\varphi - \frac{2\pi n}{N_t}\right)$ is simple expression, $f_s = 1/T_s$ is the TS-UCAs modulation frequency, $\tau_{\text{on}}^n = t_{on}^n/T_s$ and $\tau_{\text{off}}^n = t_{\text{off}}^n/T_s$ are the duty cycles of the n^{th} antenna-ON and n^{th} antenna-OFF, respectively. We can observe that the phase factor Θ_n is added to n^{th} element, and the progressive phase superpositions lead a skewing of $2\pi l$ during a whole time-switched sequence. From the Eq. (24), we can observe that the switching will leads to an unlimited expansion of the bandwidth. Specifically, unlimited harmonic signals corresponding to frequency $f + lf_s$ and mode l will be generated in theory. Fortunately, based on UCAs, only the OAM modes which satisfy $|l| \le \frac{N_t}{2}$ can be generated or received due to discrete sampling [30]. According to Eq. (25), the high order harmonic coefficients will be very small when $\tau_{\text{off}}^n - \tau_{\text{on}}^n$ is fixed, and the value of $\tau_{\text{off}}^n - \tau_{\text{on}}^n$, the duty ratio of each antenna element switch-ON, depends on the number of antenna elements at transmitter. Also, the digital filter may be an appropriate solution for bandwidth expansion.

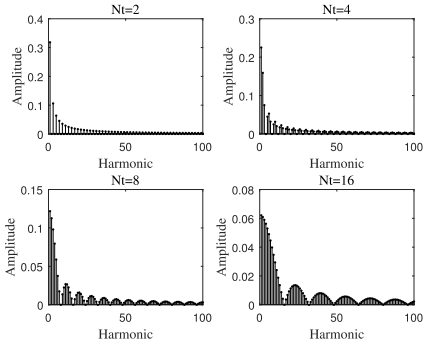

FIGURE 4. The distribution of the amplitudes corresponding to the different harmonic frequencies.

Fig. 4 also shows the distribution of the amplitudes corresponding to different harmonic frequencies for different numbers of transmitting elements N_t of 2, 4, 8, and 16, respectively. It can be observed that the duty ratio of amplitudes of the high order harmonic frequencies increases with an increase of N_t. Thus, the effect of bandwidth expansions is more evident with the N_t increasing. For an 8-element transmitter, the OFDM-OAM modulation by switches will lead an eightfold frequency expansion at least. Since there is a trade-off between the hardware simplicity and bandwidth expansion, an optimum TOO transmitter need be designed in practice. Fortunately, in a given UCA transmitter, the low order OAM signals are more suitable for transmission due to the divergence of OAM beams. Thus, a UCA with fewer elements can be used in the scheme of TOO to avoid the additional frequency expansion. For multiple different data streams, different encoding schemes such as Phase Shift Keying (PSK) and quadrature amplitude modulation (QAM) can be employed to reduce the consumption of the spectrum resources.

In the case of coaxial transmission, $e^{j\phi_n(\psi,\varphi)} = 1$ due to $\psi = 0$. For effective generated OAM modes and the m^{th} data stream, thus, the matrix form of the transmitted symbols at time-switched UCAs is given by

$$\mathbf{x}_{\text{time}}(m) = \mathbf{M}_{\text{time}}^{\text{TX}}\mathbf{P}\mathbf{s}_F(m) \tag{25}$$

with

$$\mathbf{M}_{\text{time}}^{\text{TX}} = \begin{bmatrix} e^{j\Theta_0 l_0} & e^{j\Theta_0 l_1} & \cdots & e^{j\Theta_0 l_{N_t-1}} \\ e^{j\Theta_1 l_0} & e^{j\Theta_1 l_1} & \cdots & e^{j\Theta_1 l_{N_t-1}} \\ \vdots & \vdots & \ddots & \vdots \\ e^{j\Theta_{N_t-1} l_0} & e^{j\Theta_{N_t-1} l_1} & \cdots & e^{j\Theta_{N_t-1} l_{N_t-1}} \end{bmatrix} \bullet \mathbf{A}_t \tag{26}$$

where $\mathbf{M}_{\text{time}}^{\text{TX}}$ is time-switched modulation matrix, $\mathbf{A}_t = \text{diag}([A_0, \ A_1, \ \cdots \ A_{N_t-1}])$ is the matrix of transmitting power coefficient in Eq. (24), $\mathbf{P} = \text{diag}([P_0, \ P_1, \ \cdots \ P_{N_t-1}])$ is the power allocation matrix, and $\mathbf{s}_F(m) = [s_{f_{l_0}}(m), \ s_{f_{l_1}}(m), \ \cdots s_{f_{l_{N_t-1}}}(m)]^T$ is the vector of OFDM signals with $s_{f_{l_i}}(m) = s_{l_i}(m)e^{j2\pi(f+l_i f)t}$, where $l_i \in \{-N_t/2, \cdots, 0, \cdots, N_t/2-1\}$.

We consider an eight-antenna transmitting UCAs with the radius of $r = 0.5\lambda$, where a simple time-switched sequence sequentially activates each element. Note that the time of switch-ON of the first antenna element could be any time in T_s. Fig. 5 shows the amplitude and phase profiles of TS-UCAs. It can be observed that a null area emerges in the radial direction of the amplitude profile and largens with the increase of the value of OAM eigenmode, and a progressive, uniform phase rotates with the value of $2\pi l/N_t$ in the boresight direction of the phase profile.

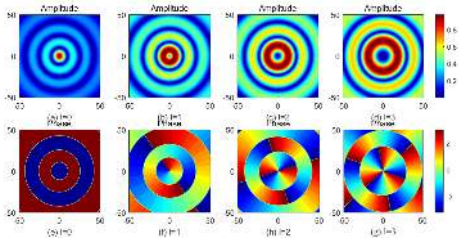

FIGURE 5. The amplitude and phase profiles of OAM waves.

2) RECEPTION AND DEMODULATION OF THE VORTEX SIGNAL

According to the description of the generation of OFDM-OAM signal in the previous subsection, the received signal corresponding to the effective receiving OAM modes is given by

$$\mathbf{y} = \mathbf{H}\mathbf{x} = \mathbf{H}\mathbf{M}_{\text{time}}^{\text{TX}}\mathbf{P}\mathbf{s}_F(m) + \mathbf{w} \tag{27}$$

where $\mathbf{y} \in^{N_r \times 1}$ is the vector of received signal and $\mathbf{w} \in^{N_r \times 1}$ is the additive white noise vector satisfying $E\{\mathbf{w}\mathbf{w}^H\} = \sigma_n^2 \mathbf{I}_{N_r}$. In the receiver, the same TS-UCAs is employed to demodulate the OFDM-OAM signal. Thus, the output vector in recive TS-UCAs is defined as

$$\mathbf{r} = \mathbf{M}_{\text{time}}^{\text{RX}}\mathbf{H}\mathbf{M}_{\text{time}}^{\text{TX}}\mathbf{P}\mathbf{s}_F(m) + \mathbf{M}_{\text{time}}^{\text{RX}}\mathbf{w} \tag{28}$$

with

$$\mathbf{M}_{\text{time}}^{\text{RX}} = \begin{bmatrix} e^{-j\Theta_0 l_0} & e^{-j\Theta_1 l_0} & \cdots & e^{-j\Theta_{N_t-1} l_0} \\ e^{-j\Theta_0 l_1} & e^{-j\Theta_1 l_1} & \cdots & e^{-j\Theta_{N_t-1} l_1} \\ \vdots & \vdots & \ddots & \vdots \\ e^{-j\Theta_0 l_{N_t-1}} & e^{-j\Theta_1 l_{N_t-1}} & \cdots & e^{-j\Theta_{N_t-1} l_{N_t-1}} \end{bmatrix} \bullet \mathbf{A}_r \tag{29}$$

where $\mathbf{M}_{\text{time}}^{\text{RX}}$ is time-switched demodulation matrix, $\mathbf{A}_r = \text{diag}([A_0, \ A_1, \ \cdots \ A_{N_r-1}])$ is the matrix of receiving power coefficient. Thus, the TSAs-based OFDM-OAM channel can be modeled as

$$\mathbf{H}_{\text{OFDM-OAM}}^{\text{TSAs}} = \mathbf{M}_{\text{time}}^{\text{RX}}\mathbf{H}\mathbf{M}_{\text{time}}^{\text{TX}} \tag{30}$$

Note that the LOS MIMO channel matrix $\mathbf{H}$ is a circulant matrix when both the transmit UCAs and the receive UCAs are placed parallel and coaxial at a distance of D (in a perfect alignment case) and are equipped with the same number of antenna elements. In this case, the distance d_{mn} only depends on the rotation angle in Eq. (2), and the number of transmitting and receiving elements satisfy $N_r = N_t = N$. Thus, the circulant matrix $\mathbf{H}$ can be diagonalized by N-point DFT matrix $\mathbf{F}_N \in^{N \times N}$. For a general case of coaxial transmission, the case of misalignment is greatly investigated in [30], where the distance d_{mn} between an arbitrary transmitting element and arbitrary receiving element has the new form

$$d_{mn} = \Big[D^2 + R_t^2 + R_r^2 + 2DR_r \sin\theta \sin\alpha - 2R_t R_r \cos\varphi \cos\theta - 2R_t R_r \sin\varphi \sin\theta \cos\alpha\Big]^{\frac{1}{2}} \tag{31}$$

where $\varphi = \left[\frac{2\pi(n-1)}{N} + \varphi_0\right]$ and $\theta = \left[\frac{2\pi(m-1)}{N} + \theta_0\right]$ are the azimuthal angles of the transmit UCAs and the receive UCAs, respectively. The unperfect alignment leads to a severe performance loss of MDM-MIMO communication systems due to the intermode interference and oblique angle receiving. The orthogonality among mutual eigenmodes was proven in [4]–[6], and this intermode interference can be completely eliminated by adopting an OAM receiver. In this paper, thus, We also need to analyze the degradation of the proposed TOO MIMO system induced by an oblique angle in the case of unperfect alignment.

D. COMPLEXITY COMPARISON

The OFDM-OAM transceiver based on baseband preprocessing, proposed by the authors of [33], performs the OFDM and OAM modulations at baseband. However, the OFDM and OAM modulations are processed at RF in the proposed TOO MIMO system, where only a switch sequence for each link needs to be designed. Moreover, the proposed TOO MIMO scheme can further reduce the computational complexity of OFDM-OAM modulation. The comparison of computational complexity is given in Table. 1.

TABLE 1. Comparison of computational complexity.

Scheme	Addition	Multiplication
Row-column FFT [33]	$MN\log_2 MN$	$\frac{1}{2}MN\log_2 MN$
2-D FFT [33]	$MN\log_2 MN$	$\frac{1}{2}MN\log_2 MN^{\frac{1}{2}}$
TSAs	MN	$M(N-1)$

III. CAPACITY ANALYSIS

According to the definition of the Laguerre-Gaussian (LG) modes [35], the expression of LG beams is given by

$$u_{lp}(r,\phi,z)=\sqrt{\frac{2r!}{[\pi\,(r+|l|)]!}}\frac{1}{w(z)}\left(\frac{\sqrt{2}r}{w(z)}\right)^{|l|}e^{-\frac{r^2}{w^2(z)}}L_p^{|l|}\times\left(\frac{2r^2}{w^2(z)}\right)e^{jk\frac{r^2}{2R(z)}}e^{-j(2r+|l|+1)\varsigma(z)}e^{jl\phi}. \quad (32)$$

in which $\varsigma(z)=\arctan\left(\frac{z}{z_R}\right)$, $w(z)=w_l\sqrt{1+z^2/z_R^2}$, and $R(z)=z\left[1+\left(\frac{\pi w_l^2}{\lambda z}\right)^2\right]$. p is the radial index; w_l and $z_R=\pi w_l^2/\lambda$ are the beam waist with OAM mode l and the Rayleigh distance, respectively; r is the size of the OAM beam; ϕ is the azimuth angle in Eq. (5); and z is the transmission distance. $L_p^{|l|}\left(\frac{2r^2}{w^2(z)}\right)$ is the generalized Laguerre polynomial. In addition, the intensity distribution is normalized such that $\int u_{lp}(r,\phi,z)\,rdrd\varphi=1$. From this expression, the size of the LG mode (which refers to the radius of the maximum beam intensity) can be calculated by solving the partial differential equation $\partial u_{lp}/\partial r=0$

$$r(u_{\max})=\sqrt{\frac{|l|}{2}}w(z). \quad (33)$$

From the above equation, we observe that this quantity $r(u_{\max})$ is not suitable for deriving the angular spread of the OAM beam due to zero value for the $l=0$ mode. Rather than the size of the LG mode, the divergence of an OAM beam depends on the standard deviation of its spatial distribution $r_{\rm rms}$ [36].

$$r_{\rm rms}(z)=\sqrt{2\pi\int_0^{\infty}r^2u_{lp}(r,\phi,z)\,rdr}=\sqrt{\frac{|l|+1}{2}}w(z). \quad (34)$$

Both $r_{\rm rms}$ and $r(u_{\max})$ mentioned previously can describe the position of the maximum OAM beam intensity in the direction of propagation, particularly a large eigenmode $|l|$. According to Eq. (33) and Eq. (34), in an arbitrarily given plane, we can observe that the size of the OAM beam increases with the increase in the value of eigenmode $|l|$ along the propagation direction. Thus, the free-space transmission gain of the higher-order eigenmode for an OAM subchannel is less than the gain of the lower-order eigenmode for an OAM subchannel in the same MDM communication system, and the capability for information transmission of OAM subchannels with different values needs to be analyzed independently.

As described in the previous section, the no inter-mode interference information transmission is the superposition of multiple OAM signals carried by different eigenmodes. To expound the procedure of independent eigenmode transmission, the received signal $y(l)$ with mode l can be written as [30]

$$y(l)=\mathbf{f}_{N_r}(l)\left(\mathbf{H}\mathbf{f}_{N_t}^H(l)\,x+\mathbf{n}\right)=h_{\rm eff}^N(l)\,x+\tilde{n}. \quad (35)$$

where $h_{\rm eff}^N(l)=\mathbf{f}(l)\,\mathbf{H}\mathbf{f}^H(l)$ is the effective OAM subchannel with eigenmode l, $\mathbf{f}_{N_t}^H(l)$ is the column vector of the N_t-point IDFT matrix $\mathbf{F}_{N_t}^H$ in the transmitter, and $\mathbf{f}_{N_r}(l)$ is the row vector of the N_r-point DFT matrix $\mathbf{F}_{N_r}$ in the receiver. Note that the received noise signal $\tilde{n}$ is still a complex Gaussian variable with zero mean and variance σ_n^2. Thanks to the mathematical derivation in [30], the approximate expressions are given as $d_{mn}=d-\frac{R_tR_r}{d}(\cos\varphi\cos\theta+\sin\varphi\sin\theta\cos\alpha)+R_r\sin\theta\sin\alpha$ and $h_{mn}=\frac{\eta}{d}\exp\left(jk\frac{R_tR_r}{d}\sin\varphi\sin\theta\cos\alpha-jkd+jk\frac{R_tR_r}{d}\cos\varphi\cos\theta-jkR_r\sin\theta\sin\alpha\right)$, where $d=\sqrt{D^2+R_t^2+R_r^2}$ is a simplified form and α is the oblique angle.

According to the definition of $h_{\rm eff}^N(l)$ in Eq. (35), the channel capacity of the signal eigenmode can be given as $C_N(l)=\log_2\left(1+p_l\left|h_{\rm eff}^N(l)\right|^2/\sigma_n^2\right)$ bits/Hz, where p_l is the transmit power allocated to the l-mode OAM signal, and σ_n^2 is the received noise variance. For simplicity, in this paper, we only focus on the case of a single link transmission where there is no inter-symbol interference. Thus, the total capacity of MDM-MIMO, OFDM-OAM MIMO, and TOO MIMO communication systems can be simplified as

$$C_{\rm total}^N=\sum_{l\in\mathcal{L}}\log_2\left(1+p_l\left|h_{eff}^N(l)\right|^2/\sigma_n^2\right)\ \text{bits/Hz}. \quad (36)$$

where $\mathcal{L}=\{l_1,\,l_2,\,\ldots,\,l_i,\,\ldots,\,l_{N-1}\}$ is the index set of selected eigenmodes with $-N/2\le l_i<N/2$. In addition, the OFDM-OAM modulation based on DFT operation and time-switched schemes are given by **Algorithm 1** and **Algorithm 2**.

Algorithm 1 The OFDM-OAM Modulation Based on DFT Operations

Initialization : $N_t, N_r, R_t, R_r, d, \lambda, \mathbf{P}$, and M.
$m=1; i=1;$
while $m\le M$ **do**
  while $l_i\le l_{N_t}$ **do**
    Obtain $\mathbf{H}$ using Eq. (3) ;
    Obtain $h_{\rm eff-DFT}^m(l_i)$ using Eqs. (15) and (35) ;
    $i=i+1;$
  end
  Obtain $C_{\rm DFT}^m$ using Eq. (36) ;
  $m=m+1;$
end
Obtain the capacity for OFDM-OAM MIMO based on DFT scheme

IV. NUMERICAL RESULTS

In this section, a LOS communication link in free space is considered for TOO MIMO, OFDM-OAM MIMO and conventional MIMO systems. On the one hand, the transmission gains of different OAM-carrying waves in TOO MIMO communication systems concerning the transmission

Algorithm 2 The OFDM-OAM Modulation Based on TS-UCAs

Initialization : $N_t, N_r, R_t, R_r, d, \lambda, \mathbf{P}, M$, and T_s.
$m = 1; i = 1; t = 0;$
while $m \leq M$ **do**
  while $l_i \leq l_{N_t}$ **do**
    while $t \leq T_s$ **do**
      Obtain $A(l_i)$ using Eq. (25) ;
      Obtain Θ_n using Eqs. (26) ;
      $t = t + T_s/N_t;$
    end
    Obtain $h^m_{\text{eff}-\text{TSA}}(l_i)$ using Eqs. (30) and (35);
    $i = i + 1;$
  end
  Obtain C^m_{TSA} using Eq. (36) ;
  $m = m + 1;$
end
Obtain the capacity for OFDM-OAM MIMO based on TS-UCAs scheme

distance are compared and analyzed. On the other hand, the channel capacities of TOO MIMO, OFDM-OAM MIMO and conventional MIMO communication systems concerning transmission distance, oblique angle, antenna spacings and SNR are considered and compared. The average energy allocation is considered for each transmitted OAM/MIMO beam to simplify the simulations. And equal numbers of antenna elements in transmitting UCAs and receive UCAs are considered. The default simulation parameters are configured as follows: λ is the wavelength, and the original antenna spacing ξ of the transmit/receive UCAs is configured as 0.5λ. The transmission SNR and transmission distance are configured as 20 dB and 30λ, respectively. The OAM states of the transmitted OAM waves are equal to the number of transmit antennas, i.e., when a 4×4 transmission array is configured, the OAM states are $l_1 = -2,\ l_2 = -1,\ l_3 = 0,\ l_4 = 1$. Note that the SE of the OFDM-OAM MIMO system is equal to the SE of the MDM-MIMO system; however, the total sum-rate of the OFDM-OAM MIMO system is M times of the total sum-rate of the MDM-MIMO system due to the multiplexing of M subcarriers.

The free-space transmission gains $|h_{ii}|^2$ of a vortex electromagnetic wave based on an 8×8 TOO MIMO system with respect to the transmission distance is evaluated in Fig. 6. In this case, $|h_{ii}|^2$ denotes the propagation gain between the i^{th} transmitting element and the i^{th} receiving element in the conventional MIMO communication system and the propagation gain of an OAM subchannel with $l{=}i$ TOO MIMO communication system. Note that the OAM eigenmode $l{=}0$ is actually the plane electromagnetic wave. Figs. 6 (a) and (b) respectively describe the transmission gains of OAM subchannels and the transmission gains of OAM normalization subchannels. As shown in Fig. 6 (a), the transmission gains decrease with increasing transmission

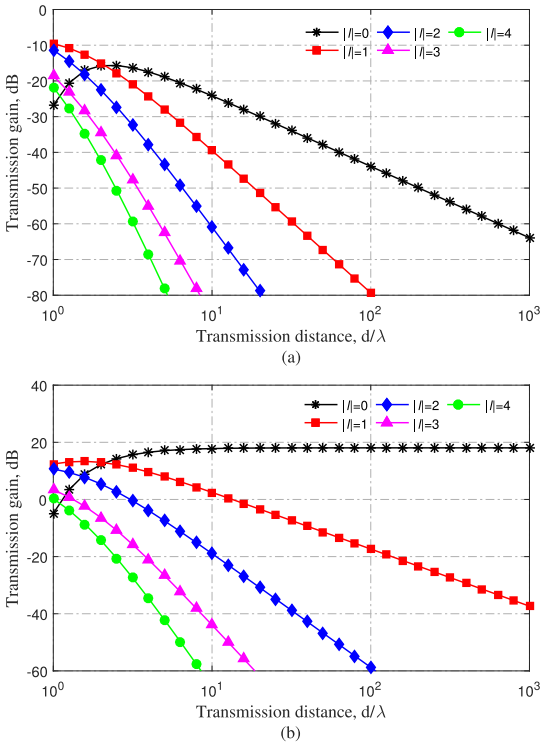

FIGURE 6. The transmission gains of $|h_{ii}|^2$ for subchannels of OAM modes $l_i = 0,\ 1,\ 2,\ 3$ and 4, respectively. (a) Transmission gains for OAM subchannels; (b) Transmission gain for normalization OAM subchannels.

distance, satisfying attenuation factor $\left(4\pi D/\lambda\right)^{2|l_i|+2}$ in far-field [37]–[39]. Moreover, the high-order OAM wave showed a lower transmission gain than the low-order OAM wave due to the more obvious divergence of the OAM wave with a larger OAM eigenmode. As shown in Fig. 6 (b), the transmission gain of plane wave (OAM eigenmode $l{=}0$) in the normalization channel showed an identical value due to eliminating the amplitude factor $\frac{\beta\lambda}{4\pi d_{ii}}$; however, the transmission gains of OAM waves still decrease with increasing transmission distance in the normalization channel, similar to the transmission gains in Fig. 6 (a). For a given aperture receiving UCA and transmission distance, the high-order vortex signals are more difficult to receive than the low-order vortex signals due to the characteristic of divergence.

Fig. 7 shows the capacities of TOO MIMO, OFDM-OAM MIMO, and conventional MIMO communication systems concerning the transmission distance considering an average power allocation scheme, and the transmit/receive UCAs are configured as 4×4 and 8×8, respectively. It can be observed that the capacities of all three MIMO communication systems decrease with increasing transmission distance. In a 4×4 configuration, the capacity of the conventional MIMO communication system is always less than the capacity of the OFDM-OAM MIMO communication system. Specifically, the capacities of OFDM-OAM MIMO and conventional MIMO communication systems decrease from their maximum values of 10.65 bit/s/Hz and 10.03 bit/s/Hz,

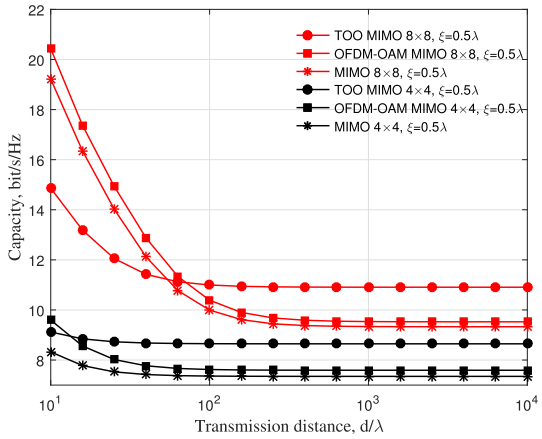

FIGURE 7. Capacities of TOO MIMO, OFDM-OAM MIMO, and conventional MIMO systems with respect to the transmission distance when $\xi = 0.5\lambda$.

respectively, to the nearly same value of 7.4 bit/s/Hz with increasing transmission distance. However, the capacity of TOO MIMO communication system is less than and then more significant than both the OFDM-OAM MIMO and conventional MIMO communication systems and keeps a considerable value of 8.65 bit/s/Hz with the increase of transmission distance. When considering an 8×8 configuration, the capacities of TOO MIMO and OFDM-OAM MIMO communication systems decrease from their maximum values of 20.43 bit/s/Hz and 19.22 bit/s/Hz, respectively, to the nearly same value of 9.3 bit/s/Hz with increasing transmission distance. Also, the capacity of the TOO MIMO communication system is less than both OFDM-OAM MIMO and a conventional MIMO communication system when the transmission distance is less than $10^2\lambda$. However, the TOO MIMO communication system obtains a better performance (10.91 bit/s/Hz) in a long transmission distance.

As shown in Fig. 8, in the 4×4 configuration, the capacities of TOO MIMO, OFDM-OAM MIMO, and conventional MIMO systems decrease with increasing transmission distance. When antenna spacing ξ is fixed, the proposed TOO MIMO system is less than and then larger than OFDM-OAM MIMO and conventional MIMO systems with the increase of transmission distance. When transmission distance d is fixed, the capacities of TOO MIMO, OFDM-OAM MIMO, and conventional MIMO systems increase with the increasing antenna spacing. When consider an 8×8 configuration, the Rayleigh distance $z_R = \frac{2(2R_t)^2}{\lambda}$ [27] increase with the increase of the number of antenna elements N_t or antenna spacing ξ. Moreover, the curves of performance comparison of the 8×8 configuration are similar to the curves of the 4×4 configuration. The system performance is relatively low in a short distance due to the energy ring of OAM waves converging with the increase of the number of antenna elements and the antenna spacing.

Fig. 9 compares the capacities of TOO MIMO, OFDM-OAM MIMO, and conventional MIMO concerning SNR considering different transmission distances. In the case

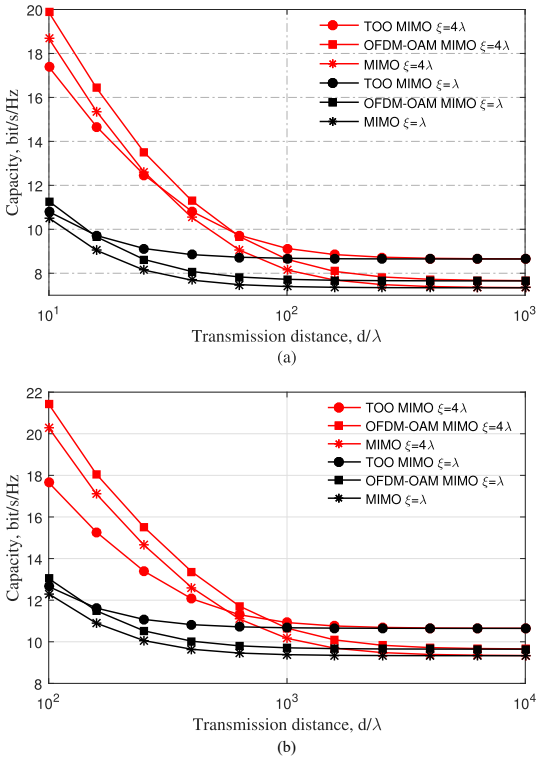

FIGURE 8. Capacities of TOO MIMO, OFDM-OAM MIMO, and conventional MIMO systems with respect to the transmission distance considering different antenna spacings. (a) 4×4 configuration; (b) 8×8 configuration.

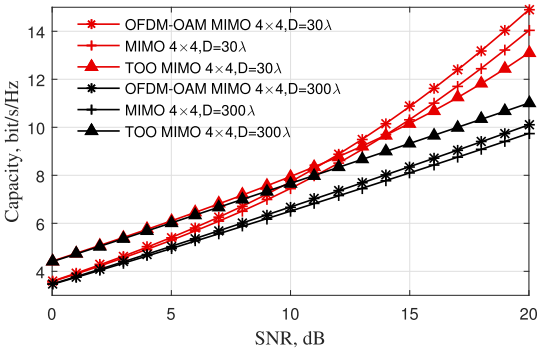

FIGURE 9. Capacities of TOO MIMO, OFDM-OAM MIMO, and conventional MIMO systems with respect to SNR considering different transmission distance.

of $D = 30\lambda$, the capabilities of all the three systems increase with the increasing SNR. Moreover, the performance of the TOO MIMO system is more significant than the performance of the OFDM-OAM MIMO and the conventional MIMO systems only when SNR $\leq$ 14dB and SNR $\leq$ 11.4dB, respectively. When the transmission distance is configured as $D = 300\lambda$, the curve of capacity concerning SNR steel keeps a positive slope. Also, the performance of the TOO MIMO system surpasses both the OFDM-OAM MIMO and conventional MIMO system at all the range of SNR.

Fig. 10 illustrates the capacity of subchannels for OAM eigenmodes $l = 1, 2$, and 3 concerning the oblique angle.

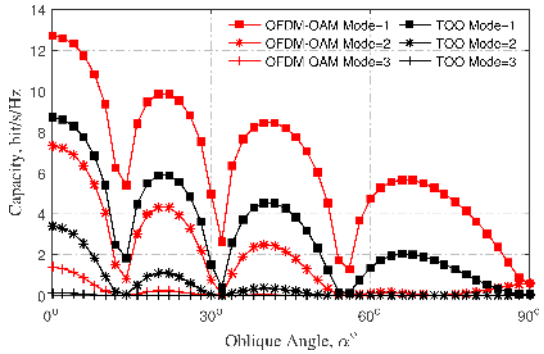

FIGURE 10. Capacity of subchannel for OAM modes $l_i = 1, 2$, and 3 of 16 × 16 TOO MIMO systems.

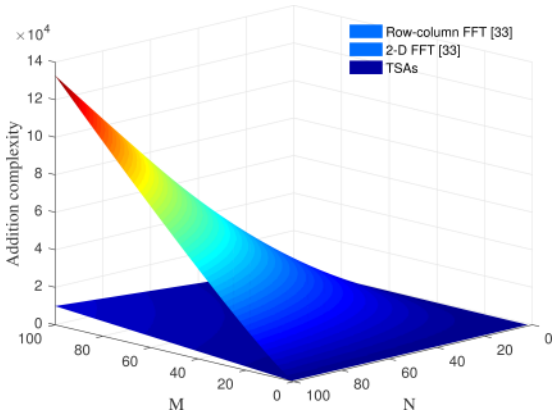

FIGURE 11. The addition complexity comparison.

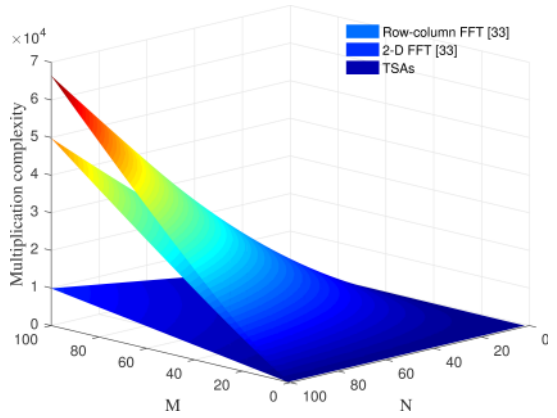

FIGURE 12. The multiplication complexity comparison.

For observation, a 16 × 16 configuration is considered. When the transmission distance is fixed, the capacity of the OAM subchannel increases with increasing number of antenna elements. It can be observed that the capacity of the OAM subchannel decreases periodically from its maximum at $\alpha = 0$ to its minimum at $\alpha = \pi/2$ and these local minima are caused by multiple phase cancellation in the receiver. In this case, the low-order eigenmodes in both TOO MIMO and OFDM-OAM MIMO are capable of strong ability in information transmission. Moreover, the proposed TOO MIMO system still has a considerable antijamming ability in the scenario of oblique angle receiving.

The complexity comparison of the addition and the multiplication of row-column FFT, 2-D FFT, and TSAs are shown in Fig. 11 and Fig. 12. We can observe that the reduction of both addition and multiplication of the proposed TSAs scheme is conspicuous due to the simple switching operations.

V. CONCLUSIONS

In this paper, the OFDM-OAM MIMO communication system is proposed and detailly derived. Moreover, the TOO MIMO communication system is then introduced to address the problem of extreme high hardware/software complexity in OFDM-OAM MIMO system, and the procedure of OAM generations and recoveries has explicitly been derived. The numerical results have shown that the TOO MIMO communication system encounters a nonnegligible performance loss in short distance due to the transmitting/receiving power coefficient matrix in TSAs. Fortunately, this performance of the TOO MIMO system approaches the optimal along with the increasing range, and the computational complexity of the proposed method is extremely low. Also, the feasibility of OAM wireless communication for short distances has been proven even in an unperfect alignment setting. For our future research, a more efficient time sequence need to be designed to improve the performance loss of the TOO MIMO system in short transmission. Besides, investigation of the solutions for the bandwidth expansion caused by switching and the exploration of the application scenarios of the TOO MIMO system will be the focus.

REFERENCES

[1] T. L. Marzetta, "Noncooperative cellular wireless with unlimited numbers of base station antennas," *IEEE Trans. Wireless Commun.*, vol. 9, no. 11, pp. 3590–3600, Nov. 2010.

[2] X. Cheng *et al.*, "Communicating in the real world: 3D MIMO," *IEEE Wireless Commun.*, vol. 21, no. 4, pp. 136–144, Aug. 2014.

[3] J. Zhang, C. Pan, F. Pei, G. Liu, and X. Cheng, "Three-dimensional fading channel models: A survey of elevation angle research," *IEEE Commun. Mag.*, vol. 52, no. 6, pp. 218–226, Jun. 2014.

[4] K. A. Opare, Y. Kuang, and J. J. Kponyo, "Mode combination in an ideal wireless OAM-MIMO multiplexing system," *IEEE Wireless Commun. Lett.*, vol. 4, no. 4, pp. 449–452, Aug. 2015.

[5] I. B. Djordjevic, "Multidimensional OAM-based secure high-speed wireless communications," *IEEE Access*, vol. 5, pp. 16416–16428, 2017.

[6] A. Tennant and B. Allen, "Generation of radio frequency OAM radiation modes using circular time-switched and phased array antennas," in *Proc. Antennas Propag. Conf. (APS)*, Jan. 2013, pp. 1–4.

[7] O. Edfors and A. J. Johansson, "Is orbital angular momentum (OAM) based radio communication an unexploited area?" *IEEE Trans. Antennas Propag.*, vol. 60, no. 2, pp. 1126–1131, Feb. 2012.

[8] W. Cheng, W. Zhang, H, Jing, S. Gao, and H. Zhang, "Orbital angular momentum for wireless communications," *IEEE Wireless Commun.*, vol. 26, no. 1, pp. 100–107, Feb. 2019.

[9] H. Jing, W. Cheng, Z. Li, and H. Zhang, "Concentric UCAs based low-order OAM for high capacity in radio vortex wireless communications," *J. Commun. Inf. Netw.*, vol. 3, no. 4, pp. 85–100, 2018.

[10] S. M. Mohammadi *et al.*, "Orbital angular momentum in radio—A system study," *IEEE Trans. Antennas Propag.*, vol. 58, no. 2, pp. 565–572, Feb. 2010.

[11] J. Wang *et al.*, "Terabit free-space data transmission employing orbital angular momentum multiplexing," *Nature Photon.*, vol. 6, no. 7, pp. 488–496, 2012.
[12] H. Huang *et al.*, "100 Tbit/s free-space data link using orbital angular momentum mode division multiplexing combined with wavelength division multiplexing," in *Proc. IEEE Opt. Fiber Commun. Conf. Expo. Nat. Fiber Optic Eng. Conf.*, Mar. 2013, pp. 1–3.
[13] T. Lei *et al.*, "Massive individual orbital angular momentum channels for multiplexing enabled by dammann gratings," *Light, Sci. Appl.*, vol. 4, no. 3, p. e257, 2015.
[14] F. Bian *et al.*, "Generation of wideband radio frequency signals carrying orbital angular momentum based on microwave photonics phase shifter," in *Proc. IEEE Laser Electro-Opt.*, Dec. 2014, pp. 1–2.
[15] M. Uchida and A. Tonomura, "Generation of electron beams carrying orbital angular momentum," *Nature*, vol. 464, no. 7289, pp. 737–739, Apr. 2010.
[16] B. Thidé *et al.*, "Utilization of photon orbital angular momentum in the low-frequency radio domain," *Phys. Rev. Lett.*, vol. 99, no. 8, 2007, Art. no. 087701.
[17] F. Tamburini, E. Mari, A. Sponselli, B. Thidé, A. Bianchini, and F. Romanato, "Encoding many channels on the same frequency through radio vorticity: First experimental test," *New J. Phys.*, vol. 14, no. 3, Mar. 2012, Art. no. 033001.
[18] J. Xu, "Degrees of freedom of OAM-based line-of-sight radio systems," *IEEE Trans. Antennas Propag.*, vol. 65, no. 4, pp. 1996–2008, Apr. 2017.
[19] Y. Yang, W. Cheng, W. Zhang, and H. Zhang, "Mode modulation for orbital-angular-momentum based wireless vorticose communications," in *Proc. IEEE Global Commun. Conf. (GLOBECOM)*, Dec. 2016, pp. 1–6.
[20] E. Cano and B. Allen, "Multiple-antenna phase-gradient detection for OAM radio communications," *Electron. Lett.*, vol. 51, no. 9, pp. 724–725, Apr. 2015.
[21] Q. Zhu, T. Jiang, Y. Cao, K. Luo, and N. Zhou, "Radio vortex for future wireless broadband communications with high capacity," *IEEE Wireless Commun.*, vol. 22, no. 6, pp. 98–104, Dec. 2015.
[22] M. Oldoni *et al.*, "Space-division demultiplexing in orbital-angular-momentum-based MIMO radio systems," *IEEE Trans. Antennas Propag.*, vol. 63, no. 10, pp. 4582–4587, Oct. 2015.
[23] Y. Ren *et al.*, "Line-of-sight millimeter-wave communications using orbital angular momentum multiplexing combined with conventional spatial multiplexing," *IEEE Trans. Wireless Commun.*, vol. 16, no. 5, pp. 3151–3161, May 2017.
[24] Y. Yuan, Z. Zhang, J. Cang, H. Wu, and C. Zhong, "Capacity analysis of UCA-based OAM multiplexing communication system," in *Proc. 5th Int. Conf. Wireless Commun. Signal (WCSP)*, Oct. 2015, pp. 1–5.
[25] Q. Zhu, T. Jiang, D. Qu, D. Chen, and N. Zhou, "Radio vortex–multiple-input multiple-output communication systems with high capacity," *IEEE Access*, vol. 3, pp. 2456–2464, 2015.
[26] W. Cheng, H. Zhang, L. Liang, H. Jing, and Z. Li, "Orbital-angular-momentum embedded massive MIMO: Achieving multiplicative spectrum-efficiency for mmWave communications," *IEEE Access*, vol. 6, pp. 2732–2745, 2017.
[27] W. Zhang *et al.*, "Mode division multiplexing communication using microwave orbital angular momentum: An experimental study," *IEEE Trans. Wireless Commun.*, vol. 16, no. 2, pp. 1308–1318, Feb. 2017.
[28] Y. Yan *et al.*, "High-capacity millimetre-wave communications with orbital angular momentum multiplexing," *Nature Commun.*, vol. 5, p. 4876, Mar. 2014.
[29] X. Ge, R. Zi, X. Xiong, Q. Li, and L. Wang, "Millimeter wave communications with OAM-SM scheme for future mobile networks," *IEEE J. Sel. Areas Commun.*, vol. 35, no. 9, pp. 2163–2177, Sep. 2017.
[30] R. Chen *et al.*, "Beam steering for the misalignment in UCA-based OAM communication systems," *IEEE Wireless Commun. Lett.*, vol. 7, no. 4, pp. 582–585, Aug. 2018.
[31] L. Wang, X. Ge, R. Zi, and C.-X. Wang, "Capacity analysis of orbital angular momentum wireless channels," *IEEE Access*, vol. 5, pp. 23069–23077, 2017.
[32] Y. Yang, W. Cheng, W. Zhang, and H. Zhang, "Mode modulation for wireless communications with a twist," *IEEE Trans. Veh. Technol.*, vol. 67, no. 11, pp. 10704–10714, Nov. 2018.
[33] R. Chen, W. Yang, H. Xu, and J. Li, "A 2-D FFT-based transceiver architecture for OAM-OFDM systems with UCA antennas," *IEEE Trans. Veh. Technol.*, vol. 67, no. 6, pp. 5481–5485, Jun. 2018.
[34] R. Bains and R. R. Müller, "Using parasitic elements for implementing the rotating antenna for MIMO receivers," *IEEE Trans. Wireless Commun.*, vol. 7, no. 11, pp. 4522–4533, Nov. 2008.
[35] M. J. Padgett, F. M. Miatto, M. P. J. Lavery, A. Zeilinger, and R. W. Boyd, "Divergence of an orbital-angular-momentum-carrying beam upon propagation," *New J. Phys.*, vol. 17, Feb. 2015, Art. no. 023011.
[36] G. Gaffoglio, A. Cagliero, A. De Vita, and B. Sacco, "OAM multiple transmission using uniform circular arrays: Numerical modeling and experimental verification with two digital television signals," *Radio Sci.*, vol. 51, no. 6, pp. 645–658, Jun. 2016.
[37] C. Craeye, "On the transmittance between OAM antennas," *IEEE Trans. Antennas Propag.*, vol. 64, no. 1, pp. 336–339, Jan. 2016.
[38] D. K. Nguyen, O. Pascal, J. Sokoloff, A. Chabory, B. Palacin, and N. Capet, "Antenna gain and link budget for waves carrying orbital angular momentum," *Radio Sci.*, vol. 50, pp. 1165–1175, Nov. 2015.

TAO HU received the B.E. degree in electronic information engineering from the China University of Geosciences (CUG), Beijing, China, in 2013, and the M.S. degree in information and communication engineering from the Chongqing University of Posts and Telecommunications (CQUPT), Chongqing, China, in 2016, where he is currently pursuing the Ph.D. degree. His research interests include orbit angular momentum wireless communications, millimeter-wave wireless communications, and multiple-input multiple-output (MIMO) wireless communications.

YANG WANG received the master's and Ph.D. degrees from The University of Sheffield, U.K., in 2011 and 2015, respectively. He joined the School of Communications and Information Engineering, Chongqing University of Posts and Telecommunications, in 2015. His research interests include antennas and propagation, radar signature management, phase-modulating microwave structures, and wireless communications.

XI LIAO received the B.S. degree in communication engineering from Hohai University, Nanjing, China, in 2011, and the Ph.D. degree in communication and information engineering from Harbin Engineering University, China, in 2015. In 2016, she joined the Department of Communication and Information Engineering, Chongqing University of Posts and Telecommunications, where she was appointed as a Lecturer, in 2016. Her current research interests include twisted radio waves and applications, antennas and radio propagation, and millimeter-wave wireless communications.

JIE ZHANG was with Imperial College London, Oxford University, and the University of Bedfordshire. Since 2011, he has been the Chair of Wireless Systems with the EEE Department, The University of Sheffield, Sheffield, U.K., where he is currently a Full Professor. He co-founded RANPLAN Wireless Network Design, Ltd., which produces a suite of world leading in-building DAS, indoor–outdoor small cell/HetNet network designs, and optimization tools iBuildNet-Professional, Tablet, DAS, and Manager. He and his students have pioneered research in femto/small cell and HetNets and published some of the earliest and most widely cited publications on these topics (three of top ten most cited). Since 2005, he has been awarded over 20 research projects by the EPSRC, the EC FP6/FP7/H2020, and industry, including some of the earliest projects on femtocell/HetNets.

QILONG SONG received the B.S. degree in electronic science and technology from the Chongqing University of Posts and Telecommunications (CQUPT), Chongqing, China, in 2016, where he is currently pursuing the M.S. degree. His research interests include orbital angular momentum waves and application in multiple-input multiple-output (MIMO) wireless communications.